analytical chemistry

Article

pubs.acs.org/ac

Liquid Crystal-Based Proton Sensitive Glucose Biosensor

Mashooq Khan and Soo-Young Park*

Department of Polymer Science & Engineering, Kyungpook National University, #1370 Sangyuk-dong, Buk-gu, Daegu 702-701, Korea

Supporting Information

ABSTRACT: A transmission electron microscopy (TEM) grid filled with 4-cyno-4-pentylbiphenyl (5CB) on the octadecyltrichloro silane-coated glass in an aqueous medium was developed to construct a glucose biosensor by coating poly(acrylicacid-b-4-cynobiphenyl-4-oxyundecylacrylate) (PAA-b-LCP) at the aqueous/5CB interface and immobilizing glucose oxidase (GOx) covalently to the PAA chains. The glucose was detected from a homeotropic to planar orientational transition of 5CB by polarized optical microscopy under crossed polarizers. The maximum immobilization density of the GOx, 1.3 molecules/nm^2 obtained in this TEM grid cell enabled the detection of glucose at concentrations as low as 0.02 mM with a response time of 10 s. This liquid crystal-based glucose sensor provided a linear response of birefringence of the 5CB to glucose concentrations ranging from 0.05 to 2 mM with a Michaelis–Menten constant (K_m) of 0.32 mM. This new and sensitive glucose biosensor has the merits of low production cost and easy detection through the naked eye and might be useful for prescreening the glucose level in the human body.

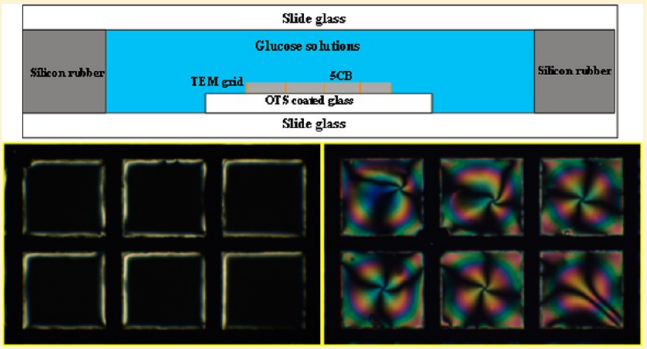

Diabetes is one of the leading causes of death and disability of millions of people worldwide. The diagnosis and management of diabetic patients requires precise monitoring and control of the glucose level in the body. Owing to the importance of glucose detection on a daily basis, a plethora of glucose biosensors have been proposed and developed over the last few decades. Until now, three generations of glucose biosensors have been developed. The first generation relies on the detection of hydrogen peroxide generated from the glucose oxidase (GOx)-catalyzed oxidation of glucose in the presence of oxygen. In the second generation, an electron acceptor (e.g., Fe(III), Mn(IV), nitrate, or sulfate) is used in combination with GOx to shuttle the generated electrons in the enzymatic reaction directly to the electrode. This electron acceptor reduces the barrier to direct electron transfer created by a thick protein surrounding the flavin adenine dinucleotide redox center of GOx. In the third generation, nonenzymatic nanocomposite electrodes using heavy metals, such as Pt, Pb, Pd, or Au, in combination with carbon nanotubes (CNTs) are used for glucose detection instead of leachable artificial mediators and GOx.[1] On the other hand, the low sensitivity, nonselective nature, high cost, and rapid loss of activity make them impractical for routine glucose analysis.[2]

Several detection methods, such as luminescence, spectroscopy, chromatography, and electrochemical analysis, have been used as glucose biosensors. Among them, the electrochemical method has attracted considerable attention owing to its good sensitivity and low detection limit.[3] The electrochemical technique measures the electrical potential generated from the oxidation of hydrogen peroxide or the reduction of oxygen at the working electrode. A major disadvantage of this glucose sensor is the high level of interference caused by the oxidation or reduction of commonly encountered compounds in clinical samples, such as uric acid (UA), acetaminophen, and ascorbic acid (AA), at the working potential.[4] To eliminate this electroactive interference, a porous membrane was used to protect the electrode. For example, an oxygen-permeable hydrophobic membrane, which excludes compounds with molecular weights greater than 100 to 200 g/mol, such as uric acid and ascorbic acid, has been used. This membrane, however, acts as a diffusion barrier that affects the detection limit, linear range, and response time. To improve the performance, CNTs, graphene, nanorods, conducting polymers, and metal nanoparticles[5] have been incorporated as a transducer. On the other hand, the rapid and reliable detection of glucose at low cost is still a challenge.

The GOx-catalyzed oxidation of glucose produces gluconic acid, which decreases the local pH, as shown in Scheme 1. Therefore, monitoring the pH can be vital in glucose analysis. Although pH sensors made from glass electrodes are readily available for monitoring the pH in aqueous solutions, they are unsuitable for measuring the pH in solutions with small volumes, as in a transmission electron microscopy (TEM) grid cell. The aim of this study was to exploit the optical properties

Received: September 12, 2013
Accepted: December 30, 2013
Published: December 30, 2013

   dx.doi.org/10.1021/ac402916v | *Anal. Chem.* 2014, 86, 1493–1501

Scheme 1. GOx-Catalyzed Oxidation of Glucose

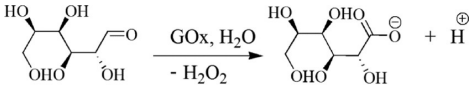

Glucose Gluconic acid

of liquid crystals (LCs) and design a label-free glucose sensor with a good spatial resolution for monitoring the changes in the localized pH, resulting from the GOx activities. LCs have a very low interfacial energy (10^{-3} to 10^{-6} J/m^2) at the LC/aqueous interface so that they are quite sensitive to environmental changes through an ordering transition, which can be propagated to a distance of ~100 μm (10^5 of molecular length).[6] The utility of LCs to transduce and amplify the molecular events at the LC/aqueous interface in response to the presence of surfactants,[7] lipids,[8] proteins,[9,10] synthetic polymers,[11−13] endotoxin,[14] simple electrolyte,[15] and the formation of a double layer by surface charges[15,16] have been reported. Moreover, when these surfactants or polymers contain pH-sensitive functional groups, the orientations of LCs become sensitive to the pH in the aqueous phase.[17] For example, the aqueous/LC interface in the TEM grid was functionalized by poly(ethylene imine) conjugated to *N*-[3-(dimethyl amino)-propyl]acrylamide) to obtain a pH-responsive LC sensor.[18] The pH-dependent change in the orientation of the LCs causing its optical appearance was attributed to changes in the chain conformation at the LC/water interface. Bi et al. developed a TEM grid pH sensor by doping 4-cyno-4-pentylbiphenyl (5CB) with 4-pentylbiphenyl-4-carboxylic acid (PBA) to visualize the local pH changes from the enzymatic hydrolysis of penicillin G by surface immobilized penicillinase. They observed a homeotropic-to-planar orientational (H−P) transition by a very small change in pH from 7.0 to 6.9. A recent report showed that a TEM grid cell functionalized with a pH-responsive amphiphilic poly(acrylicacid-b-4-cynobiphenyl-4-oxyundecylacrylate) (PAA-b-LCP) onto 5CB[10,11] exhibited a fast and reversible H−P change in 5CB in response to the swelling and shrinkage of PAA chains caused by changes in the pH of the solution.

In this paper, a glucose sensor was fabricated by immobilizing GOx on the PAA chains on a TEM grid coated with PAA-b-LCP at the 5CB/aqueous interface. In response to the pH change brought by the GOx-catalyzed oxidation of the glucose, the H−P transition of the 5CB occurred through a change in the PAA chain conformation. This LC-based TEM grid glucose sensor was tested for the low cost and simple detection of small amounts of protons produced from the enzymatic reaction with the naked eye.

EXPERIMENTAL SECTION

Materials. Microscope glass slides (Duran group, Germany) were cleaned using a piranha solution (***caution***: piranha solution is extremely corrosive and must be handled carefully), washed subsequently with distilled water, and dried under nitrogen. Copper TEM specimen grids (G75 with a grid hole width of 285 μm, pitch of 340 μm, bar width of 55 μm, size of 3.05 mm, and thickness of 18 μm) were purchased from Ted Pella, Inc., and cleaned by washing sequentially with acetic acid, acetone, and ethanol. GOx (E.C. 1.1.3.4) from *Aspergillus niger* was obtained from Sigma Aldrich as a salt-free lyophilized powder with a specific activity of >100 000 unit/g and a molecular weight of 1.6×10^5 g/mol. D(+)Glucose (Sigma), D(+)galactose (Sigma), AA (Sigma), UA (Sigma), hemoglobin (Sigma), *N*-(3-dimethylaminopropyl)-*N*-ethylcarbodiimide hydrochloride (EDC·HCl, Sigma Aldrich), *N*-hydroxysulfosuccinimide sodium salt (NHS, Sigma Aldrich), sodium chloride, trifluoroacetic acid (TFA, Aldrich, 99%), 5CB (TCI, 100%), octadecyl trichloro silane (OTS), methanol (Aldrich), and dichloromethane (DCM, Aldrich) were used as received. The amphiphilic block copolymer, PAA-b-LCP was synthesized using the same method reported previously. The molecular weight that was calculated was PAA (11K)-b-LCP (5K) with a M_w/M_n of 1.14. The Supporting Information (SI) Scheme SI 1 and Figure SI 1 present a schematic diagram of the synthesis of the block copolymer and ^{1}H NMR data, respectively.

Monolayer Formation of PAA-b-LCP. The monolayer experiments were performed with a Langmuir−Blodgett (LB) KSV Layer Builder (KSV Instruments, Ltd., AAA100178, Finland) connected to a KSV minimicro trough, which was surrounded by an environmental chamber. The working area of the trough was 17×5 cm^2. All experiments were performed at room temperature. The surface pressure of the monolayer at the air/liquid interface was measured using a Wilhelmy plate attached to a microbalance. PAA-b-LCP was dissolved in dioxane and kept at 60 °C for 2 days. Subsequently, toluene was added to the dioxane solution to obtain a final concentration of 1 mg/mL with a dioxane to toluene ratio of 6/4 (v/v). When a zero surface pressure was reached, 100 μL of a PAA-b-LCP solution was spread immediately on the water to form a monolayer. One hour after monolayer formation, the monolayer was then compressed, expanded, and compressed at a rate of 3 mm/min to achieve equilibrium. The areal density of the monolayer was controlled by the surface pressure on the spread LB film at 35 mN/m (see Figure SI 2).

Flow Cell Preparation. A homemade polydimethylsiloxane (PDMS) flow cell was made using the same method reported elsewhere.[10,11] Briefly, glass microscope slides were cleaned and coated with OTS. A copper TEM grid was placed on the surface of the 12×8 mm^2 OTS-coated glass that was glued to another common slide glass with epoxy. A 1 μL drop of 5CB was placed on a TEM grid using a 5 μL syringe. The excess 5CB was removed with a capillary tube to obtain a uniform thin film. To transfer the PAA-b-LCP monolayer onto the surface of 5CB in the TEM grid, the TEM grid filled with 5CB was inserted slowly into the PAA-b-LCP-spread trough with the TEM grid side downward coming to rest on a silicon spacer (2 mm thick) attached to another slide glass in the LB bath. The two slide glasses spaced with silicon rubber were then clipped with binder clips. The inlet and outlet ports for exchanging the solutions were made with needles that were punched through the silicon rubber. The internal volume of the flow cell was 0.4 mL. The flow cell was then flipped over and used for further analysis. Figure SI 2 shows a schematic diagram and photograph of the flow cell containing a TEM grid cell.

Immobilization of GOx to PAA. The GOx was immobilized to the PAA chains on the TEM grid using a slight modification of the method reported elsewhere.[19] Briefly, the PAA chains were activated with 0.4 M EDC·HCl and 0.1 M NHS for 1 h, and 6 mL of the GOx solution was then passed through the flow cell and kept for 12 h at room temperature, as summarized in Scheme 2.

The tested concentrations of the GOx solution (C_g) in the flow cell were 0.63, 3.13, 4.69, 6.25, 12.50, 15.63, and 18.75 μM. The concentrations of the immobilized GOx were determined spectrophotometrically with a reference sample of

dx.doi.org/10.1021/ac402916v | *Anal. Chem.* 2014, 86, 1493−1501

Scheme 2. Chemical Immobilization of the GOx to PAA Brushes

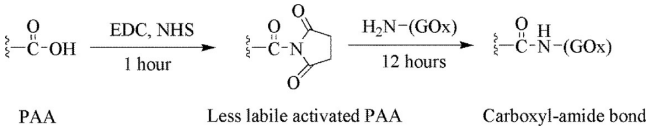

deionized water. The calibration curve for GOx (Figure SI 4) was measured in the range of 0 to 12.5 μM at a maximum absorbance wavelength (λ_{max}) of 276 nm. The amounts of immobilized GOx (C_{imb}) were calculated from the difference in the GOx solution concentration before and after immobilization.

Labeling of GOx. GOx was dissolved in a PBS buffer (pH 7.2) in a reaction vial to obtain a 15.6 μM solution into which the chemical coupling agents, EDC·HCl and NHS, were added and kept for 1 h at 4 °C to activate the carboxylic group in the GOx. Subsequently, 1 mg of Rhodamin 123 was added and stirred for 12 h at room temperature. Figure SI 5 shows the UV−vis spectrum of the GOx labeled with Rhodamin 123 ($GOx_{Rhodamin}$) with those of GOx and Rhodamin 123. The same strong absorbance at 500 nm as that of the pure Rhodamin 123 solution and blue shifting of the GOx peak from 276 to 263 nm (marked with arrows) suggested that GOx had been labeled successfully. $GOx_{Rhodamin}$ was then immobilized to the PAA using the same procedure with GOx. After immobilization, the TEM grid was washed by injecting distilled water into the flow cell to remove the unreacted Rhodamin 123.

Measurements. Images and videos of the TEM grid cells during (and after) glucose injection were recorded by polarized optical microscope (POM) (Leitz, ANA-006, Germany) under crossed polarizers using a CCD camera (Samwon, STC-TC83USB, Korea). The UV−visible spectra were obtained using a UV−visible spectrophotometer (Shimadzu, 2401, Japan). The $GOx_{Rhodamin}$ on the TEM grid was confirmed by fluorescent microscopy (Nikon Eclipse, E600POL, Japan). ^{1}H nuclear magnetic resonance (NMR, Bruker 400 MHz, Germany) analysis of the PAA-b-LCP was carried out at 400 MHz. The gray scale intensities of the frames were found by using adobe photoshop CS5. The optical birefringence (Δn) was measured using a tilting compensator (type 2073 K, equipped with a calcite compensator plate, Leitz, Germany) with the source light intensity set to 50% of full illumination. At the 0 position of the compensator, the crystal axis was parallel to the polarizer axis. Therefore, Δn is defined as Γ/d, where Γ is the phase difference and d is the sample thickness (1.8×10^4 nm). The Γ was measured from the tilting angle ($2i$) using the equation,

$$\Gamma = 10^4 f(2i) \times \frac{c}{10^4}$$

where $f(2i)$ is tabulated in the instrument manual and c is the compensator constant (4.54×10^4), as shown in Table SI 1. The measurements were made in triplicate, and the error bars represents the standard deviation (SD).

RESULTS AND DISCUSSION

Immobilization of GOx to PAA. The concentration of immobilized GOx was measured from the optical densities determined by UV−vis spectroscopy. The immobilization density of the GOx (N_{GOx}) in molecules/nm^2 was calculated using eq 1

$$N_{GOx} = \frac{C_{imb} \times N_A}{A \times M_{GOx}} \quad (1)$$

where C_{imb}, N_A, A, and M_{GOx} are the amounts of immobilized GOx in grams, Avogadro's number, area of the TEM grid in nm^2 (7.31×10^{12} nm^2), and molecular weight of GOx (1.6×10^5 g/mol), respectively. Figure 1 shows N_{GOx} as a function of the GOx concentration (C_g). The N_{GOx} increased linearly with increasing C_g until C_g = 12.5 μM and then became saturated at 1.3 molecules/nm^2. The GOx-immobilized TEM (TEM_{GOx}) grid cells were then prepared with a 12.5 μM GOx solution for further experiments.

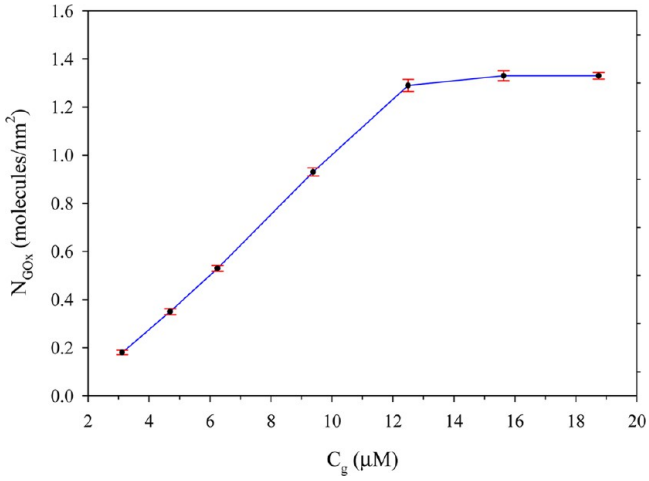

Figure 1. Plot of the N_{GOx} vs C_g.

An important parameter of the glucose sensor is the stability for a long period of time. GOx is a stable enzyme that can be stored for at least 3 months at 25 °C and for more than 6 months at 1 °C. The stability of the glucose sensor could be achieved with the immobilization of GOx by covalent bonding. Steffens et al. examined the binding of the selected proteins to the PAA brushes and correlated the binding densities with their molecular masses and sizes. The binding densities of horseradish peroxidase (HRP, 44 000 g/mol), bovin serum albumin (BSA, 66 406 g/mol), and bovin plasma fibronectin (BPF, 499 088 g/mol) were 3, 0.6, and 0.1 molecules/nm^2 respectively.[19] A protein with a high molecular weight had a lower binding density on the PAA brush. The binding density of the GOx (1.3 molecules/nm^2) was higher than that of BSA (0.6 molecules/nm^2), even though the molecular weight of GOx (1.6×10^5 g/mol) was higher than that of BSA (66 406 g/mol). The binding density of the protein is governed by the three-dimensional molecular size. For example, the molecular dimensions of BSA and dimeric GOx was $14 \times 4 \times 4$ nm^3 and $6 \times 5.2 \times 7.7$ nm^3, respectively. Therefore, BSA is more anisotropic than GOx.[20] The higher binding density of GOx in these experiments than that reported for BSA might be due to several reasons such as the anisotropic molecular shape of BSA (which occupies more space than the compact and globular GOx), the multilayered structure of the GOx, and the dimeric nature of GOx.

To confirm the immobilization of GOx on the PAA chains, $GOx_{Rhodamin}$ was immobilized on the PAA chains and observed by fluorescence microscopy. Figure 2a shows a fluorescent image of the TEM grid cell with immobilized $GOx_{Rhodamin}$. The

dx.doi.org/10.1021/ac402916v | Anal. Chem. 2014, 86, 1493−1501

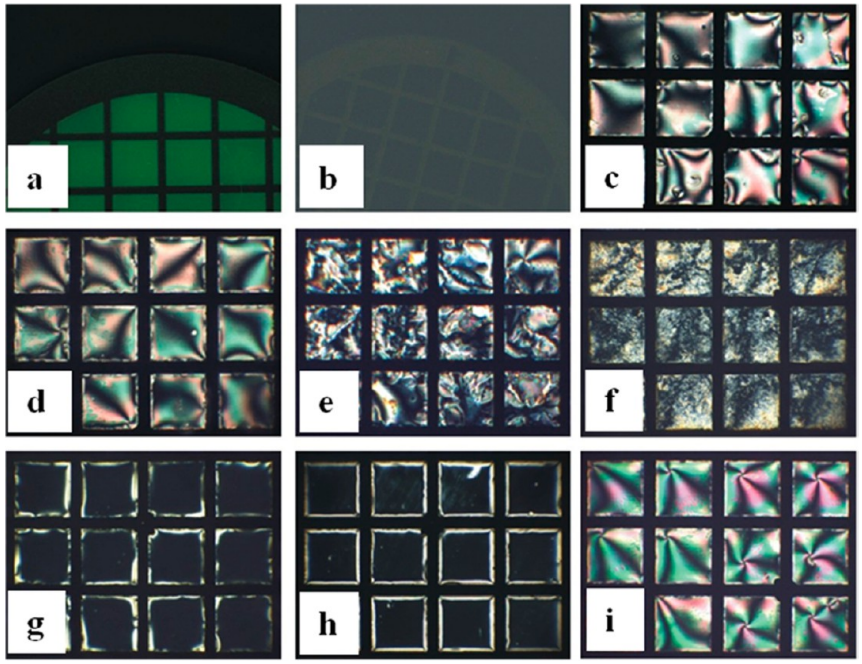

Figure 2. Fluorescent images of TEM grid cells (a) immobilized with $GOx_{Rhodamin}$ on PAA-b-LCP and (b) filled with a 15.6 μM $GOx_{Rhodamin}$ solution without a PAA-b-LCP coating; POM images of the TEM grid cells under crossed polarizers (c) with a PAA-b-LCP coating without GOx immobilization and NaCl, and those with GOx immobilization on the PAA chains at NaCl concentrations (C_{NaCl}s) of (d) 0, (e) 0.5, (f) 1.0, (g) 1.5, and (h) 2.0 M; (i) without a PAA-b-LCP coating at C_{NaCl} = 2 M.

green color was clearly observed in the region of the TEM grid, although the other regions outside of the TEM grid were almost black, indicating that GOx had been immobilized successfully on the TEM grid. For comparison, a TEM grid cell without PAA-b-LCP coating was prepared under the same conditions as those with the PAA-b-LCP coating. In this case, $GOx_{Rhodamin}$ was bound physically, not chemically, to 5CB. On the other hand, a black image (Figure 2b) was observed, indicating that the physical adsorption of GOx did not occur on 5CB in the TEM grid cell. Therefore, most of the GOx in the TEM grid cell was bound chemically to the PAA chains and could be stable for a long period of time.

Figure 2c,d show POM images of the TEM grid cells coated with a PAA-b-LCP monolayer before and after the immobilization of GOx, respectively. The planar orientation was maintained after immobilizing GOx. The challenge to this system was how to detect small amounts of H^+ ions released from the GOx-catalyzed oxidation of glucose. To detect H^+ ions from the TEM grid cell, an initial homeotropic orientation is needed before injecting the glucose solution into a flow cell to observe the H−P changes because protonation of the PAA chains by low pH solutions caused the planar orientation of the 5CB in the TEM grid cell observed in a previous study.[11,12] PAA is a weak polyelectrolyte with a pK_a of 4.7. The degree of dissociation of PAA in the bulk state is dependent on the pH, as defined by eq 2

$$\frac{1-\alpha_b}{\alpha_b} = \frac{K_a}{\rho H^+} \tag{2}$$

where α_b, K_a, and ρH^+ are the degree of dissociation in the bulk, dissociation constant and concentration of protons in solution, respectively. A high degree of dissociation at high pH results in the formation of a poly conjugate base. The pH-dependent response of PAA-b-LCP at the aqueous/LC interface were studied.[11] A planar-to-homeotropic (P−H) transition was observed with increasing pH in water. The change in the 5CB orientation might be due to the high anionic charge density of the PAA chains produced by the deprotonation of the PAA chains at high pH. The response of the LC microdroplets coated with PAA-b-LCP to changes in pH was also investigated.[12] A bipolar (planar) to radial (homeotropic) orientational change occurred with increasing pH.

The dissociation behavior of the PAA chain in the brush is complicated and dependent on the pH, salt concentration, and grafting density. Zhulina et al.[21] proposed the most popular theoretical model for the polyelectrolyte brushes. In this model, the dependence of dissociation on the salt concentration was categorized into two regimes (i.e., osmotic (OsB) and salted brush (SB) regimes). In the OsB regime (in the limit of a zero salt concentration), the proton concentration in the brush was significantly higher than in the bulk state because the exchange of dissociated protons with indifferent counterions was suppressed. As a result, the degree of dissociation in the brush was lower than that of the bulk. On the other hand, in the SB regime (at high salt concentration), the dissociation (α) is governed by eq 3:[22]

$$\alpha \approx \left(\frac{\alpha_b}{1-\alpha_b} \sigma^{-1} (\rho H^+ + \rho_s) \right)^{2/3} \tag{3}$$

where σ, α_b, and ρ_s are the grafting density, dissociation of PAA in the bulk and salt concentration, respectively. In this relationship, α increases with increasing ρ_s. Currie et al. examined the properties of the PAA brush at various salt concentrations and pH.[22] They found that at pH 3 (below the pK_a of PAA), the brush thickness was independent of the salt concentration, whereas at higher pH, the brush swelled with increasing salt concentration because of the increased charges along the chain. Mouri et al. also reported the effects of the salt concentration on the monolayer structure of an anionic

dx.doi.org/10.1021/ac402916v | Anal. Chem. 2014, 86, 1493−1501

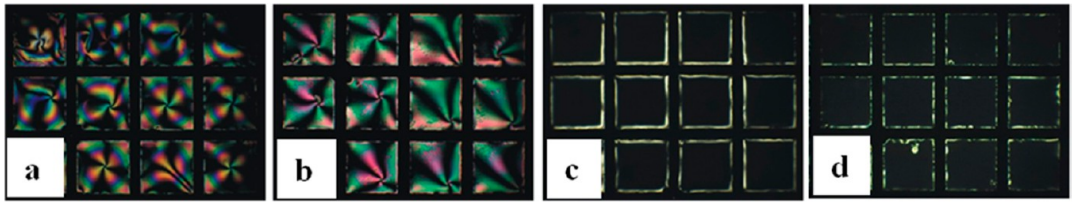

Figure 3. POM images of the TEM grid cells under crossed polarizers with (a) 3 mM glucose, (b) 1 mM acetic acid, and (c) POM image with a 3 mM glucose solution in the TEM grid cell with a PAA-b-LCP coating but without the immobilization of GOx; (d) 3 mM galactose solutions.

amphiphilic diblock copolymer of poly(diethylsilacyclobutane)-b-(methacrylic acid) (Et_2SB)-b-(PMAA) using X-ray and neutron reflectivity techniques at the air/water interface.[23] An increase in the NaCl concentration (C_{NaCl}) above 0.1 M increased the PMAA brush thickness. The change in brush thickness was attributed to the increased charge on the PMAA chain. Previous studies also reported that an increase in the charge density in the PAA chain caused the homeotropic orientation of the 5CB in the TEM grid cell. Tongbu et al. examined the effect of metal ions on the activity of GOx.[24] The GOx activity increased in the 0 to 0.5 M NaCl solutions, whereas at concentrations higher than 0.5 M, the added salts neither enhanced nor inhibited the GOx activity. In previous work, the homeotropic orientation in the TEM grid cell coated with PAA-b-LCP occurred at pH > 10. At these high pH, GOx would be denatured so that the homeotropic orientation under physiological conditions (e.g., pH = ∼7) is necessary. In this study, the initial homeotropic orientation at pH 7 was controlled by adding NaCl to the TEM grid cell.

Figure 2e−h show POM images of the TEM_{GOx} grid cells at pH 7 as a function of the C_{NaCl} in the cell. The planar orientation was observed without NaCl and at low C_{NaCl}s (0.5 and 1 M). The planar orientation at low C_{NaCl}s changed to a homeotropic orientation as C_{NaCl} was increased to 1.5 and 2 M, and the homeotropic image with a 2 M NaCl solution was darker and clearer than that with a 1.5 M NaCl solution, as shown in Figure 2g,h (also see SI movie 1). For comparison, a 2 M NaCl solution was injected into the TEM grid cell without the PAA-b-LCP coating (Figure 2i). The planar orientation did not change to a homeotropic orientation, indicating that the homeotropic orientation caused by NaCl was due to the response of the PAA chains to the added salt, not by the added salt itself. The fact that a homeotropic orientation was observed at high salt concentrations suggests an increase in the dissociation of the PAA chains with increasing salt concentration that might reach a critical value at which the 5CB in the TEM grid shows a homeotropic orientation. On the other hand, the deprotonation (or swelling of the PAA chain) might not be the only reason for altering the 5CB orientation. Recently, Carlton et al. reported the effect of NaCl on the LC orientation in the TEM grid. In their experiment, the 5CB in TEM grid was subjected to an aqueous solution of 1 M NaCl at either pH 6 or 12.8. The 5CB in contact with the 1 M NaCl solution at pH 6 exhibited a planar orientation. After replacing the solution with 1 M NaCl at pH 12.8, the initial planar orientation of 5CB in the TEM grid cell underwent a time-dependent transition in optical appearance to homeotropic ordering at the 5CB/aqueous interface. They concluded that the orientational ordering of the LC at the aqueous interface was affected strongly by the concentration of salt added to the aqueous phase due to the formation of an electrical double layer on the LC side of an LC/aqueous interface via the partitioning of ions from the aqueous phase into the LC.[15] The increase in the charge density of the PAA chains by the increased dissociation as well as double layer formation on the LC side might cause the homeotropic orientation in the TEM grid cell by adding salts in the TEM grid cell, but more studies will be needed to determine the precise role of added salts combined with weak polyelectrolytes on the LC orientation. Whatever the reasons for producing the homeotropic orientation in the TEM grid cell, an aqueous 2 M NaCl solution in water was inserted to obtain a black initial homeotropic state for further experiments.

Glucose Detection. Figure 3a shows POM images of the TEM_{GOx} grid cell at pH = 7 under the crossed polarizers by replacing the aqueous medium in the cell with a 3 mM glucose solution. The initial homeotropic orientation changed to a planar orientation.

This H−P change might be due to the release of H^+ ions in the enzymatic oxidation of the glucose, which reduced the pH in the cell and caused the protonation of the PAA chains. The pH-dependent shrinkage of PAA at the interface could alter the orientational change in the strongly anchored 5CB in the TEM grid cell. Kinsinger et al. assembled an amphiphilic block copolymer poly(ethylene imine)-b-*N*-[3-(dimethylamino)-propyl]acrylamide) at the aqueous/LC interface.[18] They observed a reversible change in the optical appearance of 5CB upon alternate exposure to pH 5 and 9 solutions, which they attributed to conformational changes (shrinkage or expansion) to the hydrophilic chains with pH. In addition, the varying charge density on the PAA chain led to a change in the 5CB orientation.[11] An acidic medium was introduced intentionally by replacing water with an acetic acid solution to determine if the H−P change occurred by lowering the pH. Figure 3b shows a POM image of the TEM_{GOx} grid cell with a 1 mM acetic acid solution (pH = 5). A similar H−P change was observed, confirming that the H−P change by the addition of glucose to the TEM_{GOx} grid cell was due to a lowering of the pH by an enzymatic reaction. Bi et al. also observed a similar response of PBA-doped 5CB confined in a penicillinase-immobilized TEM grid to H^+ ions released from the enzymatic hydrolysis of penicillin by a H−P change.[17] To confirm that the H−P change was due to the enzymatic reaction of GOx, a 3 mM glucose solution was injected into the flow cell without immobilizing GOx under otherwise similar conditions. A H−P change was not observed (Figure 3c), indicating that this H−P change was due to an enzymatic reaction of GOx.

Specificity. The specificity in a biosensor is one of the most important considerations. Therefore, the glucose sensor was tested for two monosaccharides (i.e., glucose and galactose). Both are stereoisomers with the same chemical formula ($C_6H_{12}O_6$) but different spatial arrangements of hydrogen and hydroxyl (OH) groups at carbon number 4. Figure 3d shows POM images of a TEM_{GOx} grid cell after injecting a 3

dx.doi.org/10.1021/ac402916v | *Anal. Chem.* 2014, 86, 1493−1501

mM galactose solution to the cell. The initial homeotropic orientation did not change, indicating that the TEM_{GOx} grid cell can only detect the monosaccharide in the form of glucose and is specific to the type of the monosaccharide to be detected.

Stability. Stability of TEM_{GOx} grid cell is dependent on the stability of the immobilized GOx. The denaturation of the enzyme may result in a change in the optical appearance of the 5CB and a change in the gray scale intensity. Figure 4 shows

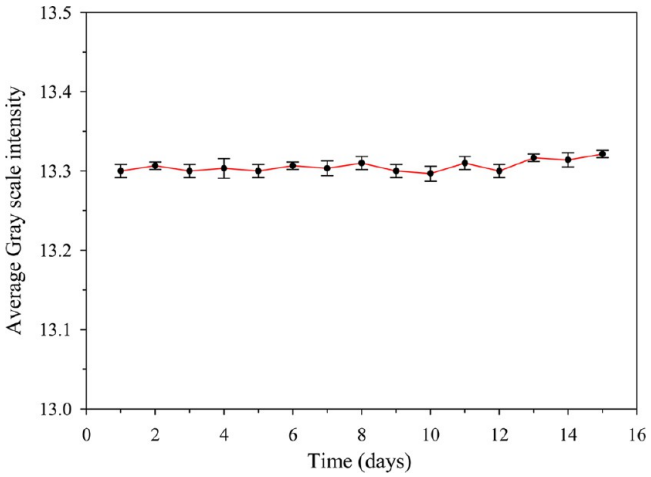

Figure 4. Average gray scale intensity vs days.

the mean gray scale intensity versus days from three different TEM_{GOx} grid cells. No significant change was observed in the gray scale intensity over 15 days. After the mentioned period of time, the TEM_{GOx} grid cells were tested for glucose detection (data not shown), and it was found that it can detect glucose the same as a freshly prepared TEM_{GOx} grid cell. Thus, the results reflects adequate stability of the TEM_{GOx} grid cell glucose sensor.

Sensitivity. Figure 5 shows POM images of the TEM grid cells with different concentrations (C_0s) of glucose solutions. The optical appearance changed with increasing C_0, and this will be discussed with the birefringence measurements in the following section. The initial homeotropic orientation did not change at $C_0 \leq 0.015$ mM (Figure 5a). With $C_0 = 0.02$ mM, a slight brightness appeared in the TEM grid cell, as shown in Figure 5b. The planar orientation became more evident as was C_0 increased (Figures 5c–f).

Under these experimental conditions, the TEM grid glucose sensor detected glucose at concentrations higher than 0.02 mM. This detection limit is low compared to many other amperometric biosensors reported in the literature.[25] Zhao et al. modified a gold electrode by depositing a layer-by-layer assembly of multiwalled carbon nanotubes (MWCNTs) coated with polydiethyldiallylammonium chloride (PDDA) and polystyrene sulfonate (PSS). The negatively charged GOx was then immobilized physically on the terminal PSS layer. They reported a detection limit of 0.058 mM. Chu et al. reported a detection limit of 0.4 mM after modifying the working electrode with GOx immobilized on CNTs in combination with Au and Pt. Hashino used CNTs with a thin plasma-polymerized film and reported a detection limit of 0.4 mM. Similarly, Monosik reported a detection limit of 0.96 mM with the nanocomposite electrode consisting of MWCNTs trapped between the chitosan layers. On the other hand, Liu and Lin reported a detection limit as low as 0.007 mM with a carbon glassy electrode modified with GOx-immobilized CNTs using a layer-by-layer method.[26] Therefore, the detection limit was lower than those from many reported glucose biosensors. This sensitive sensor, which has a low manufacturing cost, might be useful for detecting small amounts of glucose in samples by the naked eye.

Kinetics. The planar orientation of the LC provides a higher Δn than the homeotropic orientation. Therefore, the change in H–P caused a black to bright color change during the GOx reaction with glucose, as shown in SI movie 2 for $C_0 = 3$ mM. The color in the TEM grid cell observed by POM under crossed polarizers represents the retardation according to the Michel-Levy chart. The difference in the optical appearance with increasing C_0 can be an indication of the glucose level in the medium by the optical birefringence. To measure the kinetics of the GOx reaction with glucose, a measurement of Δn with time is necessary, but this measurement is quite difficult in an in situ manner with optical measurements. On the other hand, the frame of the movie represents the image in the short period (4 s), and the gray scale intensity of each clip observed by POM under crossed polarizers can represent the birefringence, even though there is no linear relationship between them. Figure 6 shows the gray scale intensity as a function of time at different C_0s. When C_0 was high, the gray

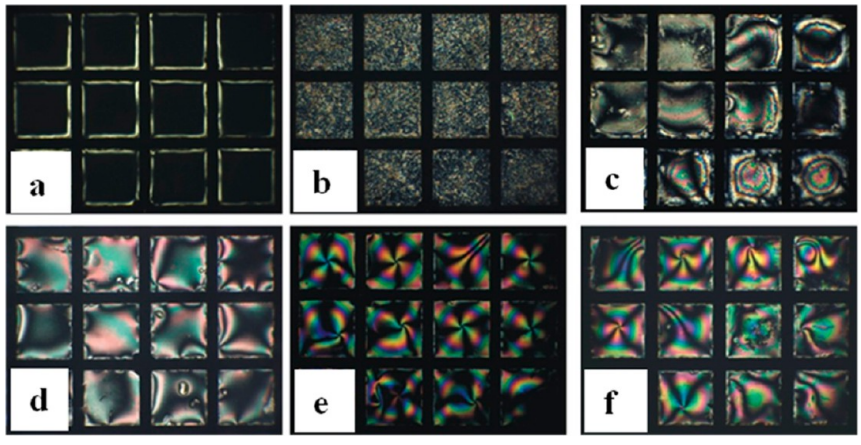

Figure 5. POM images of the TEM grid cells under crossed polarizers with different glucose concentrations (C_0) of (a) ≤ 0.015, (b) 0.02, (c) 0.05, (d) 0.5, (e) 3, and (f) 6 mM.

dx.doi.org/10.1021/ac402916v | *Anal. Chem.* 2014, 86, 1493–1501

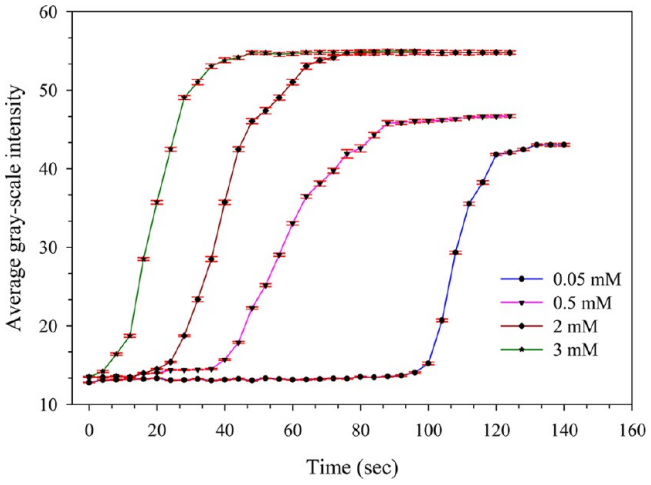

Figure 6. Average gray scale intensity as a function of time at different C_0s.

scale intensity increased rapidly to the saturation level, whereas when C_0 is low, the gray scale intensity increased slowly to the saturation level. The times for reaching half of the saturated level were 108, 59, 36, and 20 s at C_0 = 0.05, 0.5, 2, and 3 mM, respectively. The saturation level also increased with increasing C_0.

From the gray scale measurements with time, the speed of the change in the birefringence and its final saturated value is dependent on the amount of glucose present in the cell. This is quite important because the TEM grid cell can detect glucose, not only in an on−off manner but also quantitatively by measuring the birefringence. Therefore, precise measurements of the birefringence are quite important. The Δn values of the TEM grid glucose sensor were measured for different C_0s, ranging from 0.05 to 6 mM. The mechanism of the GOx-catalyzed reaction were studied using the Michaelis−Menten equation, which is the best-known model for the enzyme kinetics, as governed by eq 4 with modifications by changing the v to Δn and V_{max} to Δn_{max}

$$\Delta n = \frac{\Delta n_{max} C_0}{K_m + C_0} \tag{4}$$

where Δn_{max} and K_m are the maximum birefringence achieved at the saturated level of the substrate, and the Michaelis−Menten constant represents the inverse sensitivity of Δn vs C_0, respectively. A low K_m value represents the high sensitivity of Δn versus C_0. Figure 7a shows the change in Δn as a function of C_0. The Δn varied linearly until C_0 = 2 mM and became saturated at ∼0.08 and higher.

The data in Figure 7a can be replotted according to the linear form of the Michaelis−Menten kinetics equation, as shown in eq 5

$$\frac{C_0}{\Delta n} = \frac{K_m}{\Delta n_{max}} + \frac{1}{\Delta n_{max}} C_0 \tag{5}$$

From the intercept and slope of the plot of $(C_0/\Delta n)$ versus C_0 (Figure 7b), the K_m and Δn_{max} were 0.32 and 0.084, respectively. The K_m value, 0.32, was smaller than the 3.94, 14, and 4.3 mM reported in the literature.[27,28] The small K_m value suggests that the GOx immobilized to the PAA chains in the TEM grid cell were more sensitive to glucose than that in the other studies. The linear range of the TEM glucose sensor

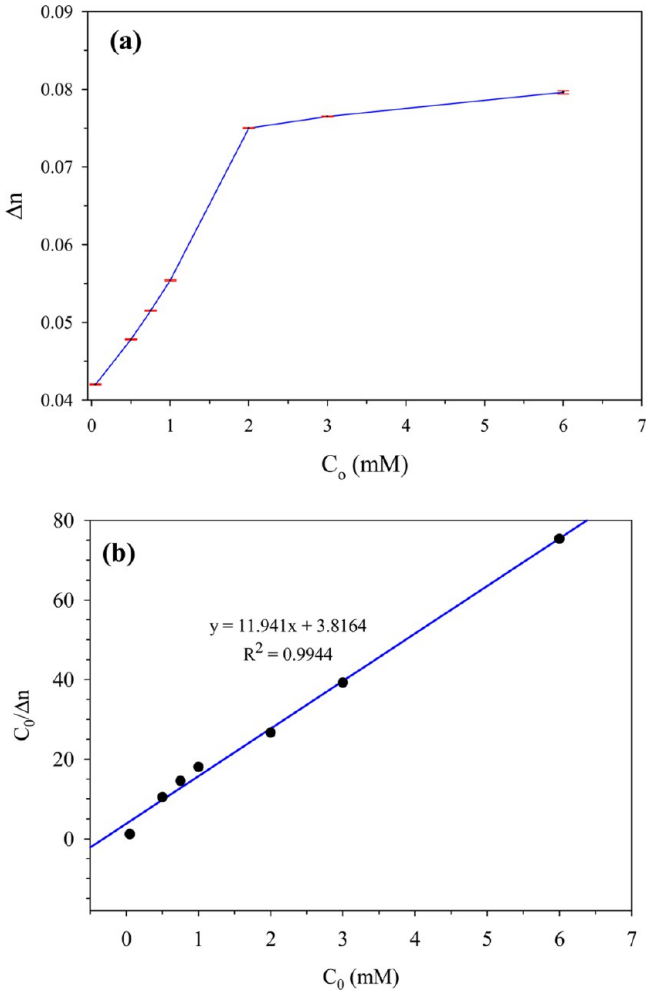

Figure 7. Plots of (a) Δn and (b) $(C_0/\Delta n)$ as a function of C_0.

(0.05−2 mM) is comparable to most of the reported data. For example, Jing-Juan et al.,[27] Liu et al.,[26] and Zhai et al.[29] reported values ranging from 0.05 to 3, 0.015 to 6, and 0.01 to 8 mM, respectively. The Δn_{max} is due to the maximum parallel orientation obtainable in this TEM grid cell. In the TEM grid cell geometry, the liquid crystals at the bottom part are always in contact with the OTS-coated glass so that the liquid crystals are always perpendicular to the glass, which gives a homeotropic orientation and a low Δn. The bright color of the TEM grid cell was attributed to the parallel orientation of the liquid crystals at the upper part of the cell that is in contact with water. Therefore, the overall orientation would be the result of a continuous change from homeotropic to planar in the cell so that Δn_{max} represents the maximum Δn. This overall orientation can be achieved when the upper part of the cell is in a perfect parallel orientation and is dependent on the conditions for fabricating the TEM grid cell, such as the hydrophobicity of the OTS-coated glass, brush density and composition of the PAA-b-LCP, the density of the immobilized GOx, and so forth.

Response of TEM_{GOx} to Blood Solutions. A blood sample of 1 mL from a healthy donor was taken in a vial and diluted 10, 100, 250, 500, and 1000× with distilled water. (*Note: To avoid microbial activity, vials were first treated with UV for 15 min*). Figure 8 shows the response of TEM_{GOx} to the blood solutions. No H−P change was observed with 1000 and

dx.doi.org/10.1021/ac402916v | *Anal. Chem.* 2014, 86, 1493−1501

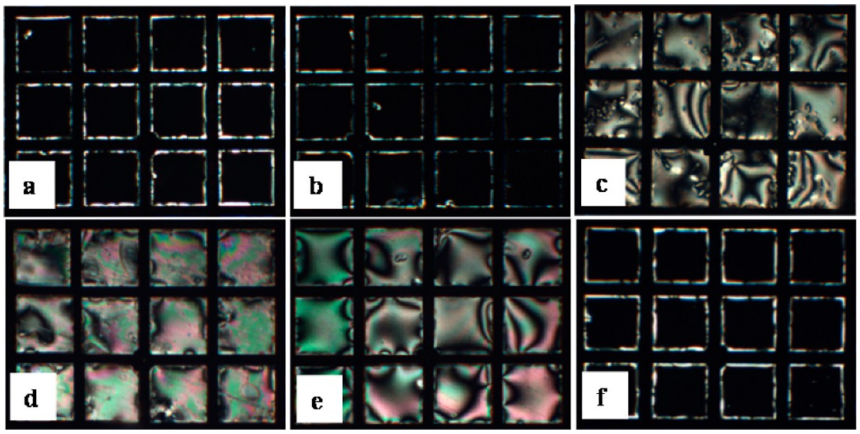

Figure 8. POM images of the TEM_{GOx} under crossed polarizers in blood samples with (a) 1000, (b) 500, (c) 250, (d) 100, and (e) 10× dilutions and (f) a 0.1 wt % hemoglobin aqueous solution.

500× dilutions (Figures 8a,b). A H−P change was observed with a 250× dilution (Figure 8c), and the H−P change became visible with 100 and 10 × dilutions (Figure 8d,e). Blood is known to contain a lot of hemoglobin in the red blood cell, which may affect the H−P change. In order to confirm the effect of the hemoglobin on the H−P change, a 0.1 wt % hemoglobin solution was tested (Figure 8f); 0.1 wt % is higher than the concentration of the hemoglobin in the tested blood with dilution. The initial homeotropic configuration remained, indicating that hemoglobin did not affect the H−P orientation. Besides, the other common electro-active species such as AA and UA present in the blood may interfere with the glucose detection. The level of the AA and UA in the blood is about 0.1 and 0.3 mM, respectively. Figure 9 shows the response of

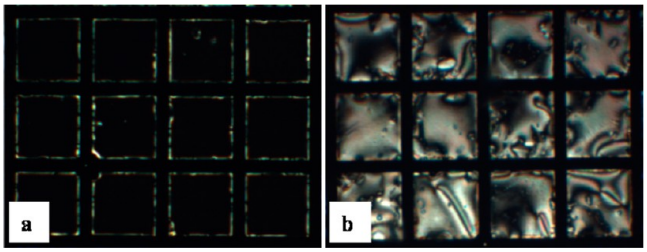

Figure 9. POM images of the TEMGOx grid cell under crossed polarizers in a solution of AA(0.015 mM), UA (0.035 mM), and glucose (a) 0.01 and (b) 0.05 mM.

TEM_{GOx} to the mixture solution of the AA, UA, and glucose. A 0.015 mM mixture solution (0.0015 mM AA, 0.0035 mM UA, and 0.01 mM glucose) was injected into the TEM_{GOx} grid cell, no H−P change was observed (Figure 9a). These particular concentrations of the AA and UA were used because this is the maximum possible concentrations for both acids in the blood at a 100× dilution of the blood. To find the interference from AA and UA, the glucose concentration was increased to 0.05 mM in the mixture (Figure 9b). The value of Δn obtained from Figure 9b was 0.0429 ± 0.00005, which increases only 2% from the Δn from the pure glucose (0.0420 ± 0.00005) at C_0 = 0.05 mM (see SI Table 1). This effect may be minimized with the choice of a proper buffer solution for this system. Although the effects of many other components in the blood on the H−P change should be studied, the present data suggest that the TEM_{GOx} may provide enough specificity for prescreening of the glucose from the blood.

CONCLUSION

A TEM grid filled with 5CB on an OTS-coated glass substrate was used to construct a reliable, fast, and proton-sensitive glucose biosensor by coating with PAA-b-LCP at the water/LC interface and immobilizing GOx on the PAA chains through covalent bonding between them. This LC-based glucose biosensor could detect small amounts of glucose in a sample with high sensitivity. The LC-based TEM grid cell functionalized with GOx-immobilized PAA-b-LCP showed a linear range of Δn against the glucose concentration, covalent bonding of GOx, small K_m value, short response time, long-term stability, and selective detection of glucose against galactose. Therefore, this biosensor cell can be used in the quantitative and specific measurement of glucose with high activity and sensitivity. These performance properties might open a different way for glucose sensing using the unique high sensitivity of liquid crystals against external stimuli. Without sophisticated instruments for glucose sensing, this highly sensitive LC-based new glucose sensor is expected to allow the fabrication of cost-effective and effectively detecting (with naked eyes) glucose sensors for commercial applications.

ASSOCIATED CONTENT

Supporting Information

Synthesis of PAA-b-LCP, ^{1}H NMR spectrum of PAA-b-LCP, LB isotherm curve of the PAA-b-LCP monolayer on water, schematic diagram and photograph of the flow cell containing a TEM grid cell, standard callibaration curve of GOx, UV−vis spectra of GOx $GOx_{Rhodamin}$ and Rhodamin 123, compensator reading and calculation of Δn, real-time video of P−H transition of the TEM_{GOx} with 2 M NaCl, and real-time video of H−P transition of the TEM_{GOx} with 3 mM glucose. This material is available free of charge via the Internet at http://pubs.acs.org.

AUTHOR INFORMATION

Corresponding Author

*E-mail: psy@knu.ac.kr.

Notes

The authors declare no competing financial interest.

ACKNOWLEDGMENTS

This work was supported by the National Research Foundation of Korea (NRF-2011-0020264).

REFERENCES

(1) Zhu, Z.; Garcia-Gancedo, L.; Flewitt, A. J.; Xie, H.; Moussy, F.; Milne, W. I. *Sensors* **2012**, *12*, 5996−6022.
(2) Rahman, M. M.; Ahammad, A. J. S.; Jin, J.-H.; Ahn, S. J.; Lee, J.-J. *Sensors* **2010**, *10*, 4855−4886.
(3) Rad, A. S.; Mirabi, A.; Binaian, E.; Tayebi, H. *Int. J. Electrochem. Sci.* **2011**, *6*, 3671−3683.
(4) Cai, Q.; Zeng, K.; Ruan, C.; Desai, T. A.; Grimes, C. A. *Anal. Chem.* **2004**, *76*, 4038−4043.
(5) Lu, J.; Do, I.; Drzal, L. T.; Worden, R. M.; Lee, I. *ACS Nano* **2008**, *2*, 1825−1832.
(6) Bai, Y.; Abbott, N. L. *J. Am. Chem. Soc.* **2012**, *134*, 548−558.
(7) Luk, Y.-Y.; Abbott, N. L. *Curr. Opin. Colloid Interface Sci.* **2002**, *7*, 267−275. Brake, J. M.; Mezera, A. D.; Abbott, N. L. *Langmuir* **2003**, *19*, 6436−6442.
(8) Brake, J. M.; Daschner, M. K.; Luk, Y. Y.; Abbott, N. L. *Science* **2003**, *302*, 2094−2097.
(9) Gupta, V. K.; Skaife, J. J.; Dubrovsky, T. B.; Abbott, N. L. *Science* **1998**, *279*, 2077−2080. Jang, C. H.; Tingey, M. L.; Korpi, N. L.; Wiepz, G. J.; Schiller, J. H.; Bertics, P. J.; Abbott, N. L. *J. Am. Chem. Soc.* **2005**, *127*, 8912−8913.
(10) Seo, J. M.; Khan, W.; Park, S.-Y. *Soft Matter* **2012**, *8*, 198−203.
(11) Lee, D. Y.; Seo, J. M.; Khan, W.; Kornfield, J. A.; Kurjib, Z.; Park, S. Y. *Soft Matter* **2010**, *6*, 1964−1970.
(12) Khan, W.; Choi, J. H.; Kimb, G. M.; Park, S. Y. *Lab Chip* **2011**, *11*, 3493−3498.
(13) Kinsinger, M. I.; Buck, M. E.; Abbot, N. L.; Lynn, D. M. *Langmuir* **2010**, *26*, 10234−10242. Khan, W.; Seo, J.-M.; Park, S. Y. *Soft Matter* **2011**, *7*, 780−787.
(14) Miller, D. S.; Abbott, N. L. *Soft Matter* **2013**, *9*, 374−382.
(15) Carlton, R. J.; Gupta, J. K.; Swift, C. L.; Abbott, N. L. *Langmuir* **2012**, *28*, 31−36.
(16) Shah, R. R.; Abbott, N. L. *J. Phys. Chem. B* **2001**, *105*, 4936−4950.
(17) Bi, X.; Hartono, D.; Yang, K.-L. *Adv. Funct. Mater.* **2009**, *19*, 3760−3765.
(18) Kinsinger, M. I.; Sun, B.; Abbott, N. L.; Lynn, D. M. *Adv. Mater.* **2007**, *19*, 4208−4212.
(19) Steffens, G. C. M.; Nothdurft, L.; Buse, G.; Thissen, H.; Höcker, H. H.; Klee, D. *Biomaterials* **2002**, *23*, 3523−3531.
(20) (a) Wright, A. K.; Thompson, M. R. *Biophys. J.* **1975**, *15*, 137−141. (b) Libertino, S.; Aiello, V.; Scandurra, A.; Renis, M.; Sinatra, F. *Sensors* **2008**, *8*, 5637−5648.
(21) Zhulina, E. B.; Borisov, O. V.; Birshtein, T. M. *Macromolecules* **1999**, *32*, 8189−8196.
(22) Currie, E. P. K.; Sieval, A. B.; Fleer, G. J.; Stuart, C. M. A. *Langmuir* **2000**, *16*, 8324−8333.
(23) Mouri, E.; Kaewsaiha, P.; Matsumoto, K.; Matsuoka, H.; Torikai, N. *Langmuir* **2004**, *20*, 10604−10611.
(24) Tongbu, L.; Xinyu, P.; Huiying, Y.; Liangnian, J. *Enzyme Microb. Technol.* **1996**, *19*, 339−342.
(25) (a) Zhao, H.; Ju, H. *Anal. Biochem.* **2006**, *350*, 138−144. (b) Chu, X.; Duan, D.; Shen, G.; Yu, R. *Talanta* **2007**, *71*, 2040−2047. (c) Monosik, R.; Stredansky, M. S.; Luspai, K.; Magdolen, P.; Sturdik, E. *Enzyme Microb. Technol.* **2012**, *50*, 227−232.
(26) Liu, G.; Lin, Y. *Electrochem. Commun.* **2006**, *8*, 251−256.
(27) Jing-Juan, X.; Hong-Yuan, C. *Anal. Biochem.* **2000**, *280*, 221−226.
(28) Malitesta, C.; Palmisano, F.; Torsi, L.; Zambonin, P. G. *Anal. Chem.* **1990**, *62*, 2735−2740. Zhang, S.; Wang, N.; Yu, H.; Niu, Y.; Sun, C. *Bioelectrochemistry* **2005**, *67*, 15−22.
(29) Zhai, D.; Liu, B.; Shi, Y.; Pan, L.; Wang, Y.; Li, W.; Zhang, R.; Yu, G. *ACS Nano* **2013**, *7*, 3540−3546.